Article

Quantitative Angle-Resolved SPR Imaging of DNA–DNA and DNA–Drug Kinetics

Lauren K. Wolf, Dominic E. Fullenkamp, and Rosina M. Georgiadis

J. Am. Chem. Soc., **2005**, 127 (49), 17453-17459• DOI: 10.1021/ja056422w • Publication Date (Web): 16 November 2005

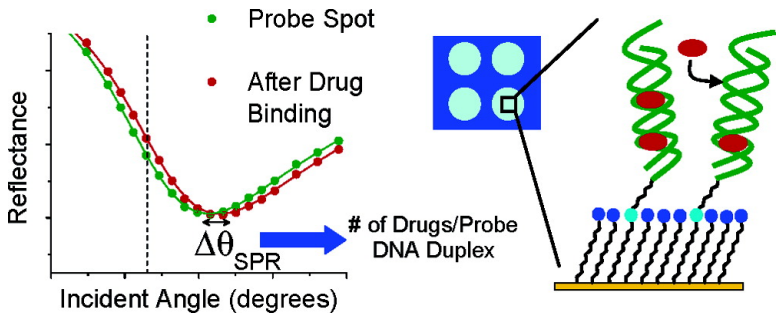

More About This Article

Additional resources and features associated with this article are available within the HTML version:

- Supporting Information
- Links to the 18 articles that cite this article, as of the time of this article download
- Access to high resolution figures
- Links to articles and content related to this article
- Copyright permission to reproduce figures and/or text from this article

View the Full Text HTML

J|A|C|S
ARTICLES
Published on Web 11/16/2005

Quantitative Angle-Resolved SPR Imaging of DNA−DNA and DNA−Drug Kinetics

Lauren K. Wolf, Dominic E. Fullenkamp, and Rosina M. Georgiadis*

Contribution from the Department of Chemistry, Boston University, 590 Commonwealth Avenue, Boston, Massachusetts 02215

Received September 18, 2005; E-mail: rgeorgia@bu.edu

Abstract: We demonstrate the quantitative characterization of DNA−DNA and DNA−drug interactions by angle-resolved surface plasmon resonance (SPR) imaging. Combining the angle-scanning capabilities of traditional SPR with the spatial definition capabilities of imaging, we directly measure DNA and drug surface coverages and kinetics simultaneously for multiple patterned spots. We find excellent agreement of DNA−DNA hybridization kinetics and thermodynamics measured by both the imaging system and traditional SPR. Instrument response and sensitivity is further demonstrated by successful measurement of association and dissociation kinetics of actinomycin-D binding to a low-density doubled-stranded DNA binding sequence. Without independent calibration, analysis of angle-resolved SPR imaging data yields 2.9 ± 0.1 drugs per duplex at saturation coverage, consistent with all available duplex binding sites being occupied.

Introduction

Currently, there is a great demand for array-based techniques capable of measuring the kinetics and thermodynamics of biomolecule interactions. In particular, surface plasmon resonance (SPR) imaging has emerged as a label-free method for the in situ investigation of such biological systems. Since the pioneering work of Knoll and others,[1,2] SPR imaging has gained popularity and, in recent years, been applied to the study of multiplexed DNA−DNA,[3−5] DNA−protein,[6] and protein−protein[7] interactions. Corn and co-workers have developed patterning techniques, attachment chemistries, and detection schemes to improve the overall quality and sensitivity of SPR imaging.[8,9] In addition, Campbell and co-workers have recently developed a calibration-based method for low accuracy quantitative image analysis.[10] Despite these advances, SPR imaging remains quantitatively limited compared to traditional angle-scanning SPR spectroscopy, which provides absolute molecular surface coverage when combined with Fresnel optical model fitting.

While, in principle, SPR imaging can be used for quantitative analysis, in practice, most applications employ fixed-angle rather than multi-angle imaging and rely on independent thickness or coverage measurements by methods such as ellipsometry[11] or fluorescence spectroscopy.[4] Campbell and co-workers rely on convenient calibration curves for direct quantitation by SPR, but are limited by an inherently low absolute accuracy (±35%) in molecular layer thickness determination.[10] As a result, most imaging techniques are currently limited to making relative affinity measurements.

SPR imaging is also limited by surface molecular architecture. Because SPR detects molecular surface adsorption based on a local change in refractive index, there is no inherent discrimination between specific and nonspecific binding events. For imaging to be effective, chemistries must be developed that allow the molecular interaction of interest, while blocking all other nonspecific surface interactions. Most researchers correct for such nonspecific interactions with a background or reference channel, but this background subtraction can have significant effects on kinetic and thermodynamic results, particularly for low-density probe surfaces.[12]

We have developed an angle-scanning SPR imaging instrument for the measurement and characterization of absolute submonolayer molecular coverages. Quantitation is enabled by the collection of polarization- and angle-resolved images, which are used for correction of light source intensity variation and optical model fitting, respectively. In this way, we provide accurate measurements of surface coverage without the need for instrumental calibration. We have selected a surface molecular architecture that efficiently blocks the nonspecific surface binding of both DNA and smaller molecules of interest. Using standard surface chemistry that has been previously applied to

(1) Rothenhäusler, B.; Knoll, W. *Nature* **1988**, *332*, 615−617.
(2) Yeatman, E.; Ash, E. A. *Electron. Lett.* **1987**, *23*, 1091−1092.
(3) Thiel, A. J.; Frutos, A. G.; Jordan, C. E.; Corn, R. M.; Smith, L. M. *Anal. Chem.* **1997**, *69*, 4948−4956.
(4) Nelson, B. P.; Grimsrud, T. E.; Liles, M. R.; Goodman, R. M.; Corn, R. M. *Anal. Chem.* **2001**, *73*, 1−7.
(5) Bassil, N.; Maillart, E.; Canva, M.; Levy, Y.; Millot, M. C.; Pissard, S.; Narwa, W.; Goossens, M. *Sens. Actuators, B* **2003**, *94*, 313−323.
(6) Shumaker-Parry, J. S.; Zareie, M. H.; Aebersold, R.; Campbell, C. T. *Anal. Chem.* **2004**, *76*, 918−929.
(7) Wegner, G. J.; Wark, A. W.; Lee, H. J.; Codner, E.; Saeki, T.; Fang, S. P.; Corn, R. M. *Anal. Chem.* **2004**, *76*, 5677−5684.
(8) Brockman, J. M.; Frutos, A. G.; Corn, R. M. *J. Am. Chem. Soc.* **1999**, *121*, 8044−8051.
(9) Goodrich, T. T.; Lee, H. J.; Corn, R. M. *Anal. Chem.* **2004**, *76*, 6173−6178.
(10) Shumaker-Parry, J. S.; Campbell, C. T. *Anal. Chem.* **2004**, *76*, 907−917.
(11) Pyo, H. B.; Shin, Y. B.; Kim, M. G.; Yoon, H. C. *Langmuir* **2005**, *21*, 166−171.
(12) Ober, R. J.; Ward, E. S. *Anal. Biochem.* **1999**, *271*, 70−80.

Table 1. Oligonucleotide Sequences

oligonucleotide	sequence
P	$H_2N-(CH_2)_6-$5′-AGATCAGTGCGTCTGTACTAGCACA-3′
C	3′-TCTAGTCACGCAGACATGATCGTGT-5′
CN	3′-ACACGATCATGTCTGCGTGACTAGA-5′
D	$H_2N-(CH_2)_6-$5′-TTTTGCTAATATGCTATAATGCTAT-3′
DC	3′-AAAACGATTATACGATATTACGATA-5′
poly(dT)	$H_2N-(CH_2)_6-$5′-$(T)_{25}$-3′

the printing of protein patterns,[13] we link amine-terminated DNA to a passive layer of mercaptoundecanoic acid and pattern without the need for robotic instrumentation. We find excellent agreement in the kinetics and thermodynamics of DNA hybridization measured by our newly developed SPR imaging system and traditional angle-scanning techniques. In addition, we present multiplexed SPR imaging results for DNA−drug (smaller molecule) interactions, demonstrating the sensitivity of our system.

Materials and Methods

Materials. All oligonucleotides were purchased from Integrated DNA Technologies (IDT). The HPLC-purified 5′ amine-terminated 25-mers and their PAGE-purified complements were used as received. These sequences and their abbreviations are listed in Table 1.

Actinomycin-D (ACTD) from Sigma was dissolved in methanol (Aldrich, spectrophotometric grade) before use. *N*-Hydroxysuccinimide (NHS) (Aldrich), *N*-(3-dimethylaminopropyl)-*N*′-ethylcarbodiimide hydrochloride (EDC) (Sigma), and mercaptoundecanoic acid (Aldrich) were used as received for surface fabrication. Self-assembly of mercaptoundecanoic acid (MUA) onto gold surfaces was carried out in ethanol (Aldrich, ACS grade). Amine-terminated DNA sequences were dissolved in 0.1 M NaCl/phosphate buffer solutions (25 mM sodium phosphate, pH ∼8.6) for hand-spotting. Angle-resolved imaging, DNA hybridizations, and drug binding experiments were carried out in 1 M NaCl/TE (TE = 10 mM Tris, 1 mM EDTA, pH ∼7.6) buffer solution. All salts were obtained from Sigma (SigmaUltra grade) and dissolved in 18 MΩ·cm distilled water. Sodium dodecyl sulfate (SDS) (Sigma-Aldrich), 0.4 wt %, was used for surface regeneration.

Surface Fabrication. Surfaces for studying DNA hybridization or DNA−drug binding with SPR imaging were prepared on SF-10 glass slides (18 × 18 mm, GenTel BioSurfaces, Inc.). These slides were cleaned with "piranha solution" (7:3 H_2SO_4/H_2O_2 (30% solution)) at >50 °C for 20 min, rinsed with distilled water, and dried under nitrogen prior to evaporation. Thermal evaporation of ∼10 Å chromium (R.D. Mathis Company) followed by ∼450 Å gold (Kurt J. Lesker Inc., 99.99%) was then carried out at pressures of $(2-5) \times 10^{-6}$ Torr.

Prior to surface treatment, the gold-coated slides were again cleaned with piranha solution for 5 min, rinsed with distilled water, and dried under nitrogen. These bare gold-coated slides were immediately immersed in 2 mM MUA in ethanol. After overnight immersion, the MUA-coated surfaces were rinsed with copious amounts of ethanol and water, soaked in ethanol for 20 min, rinsed again with water, and dried under nitrogen. The slides were then exposed to an aqueous solution containing 0.05 M NHS and 0.2 M EDC for 30−40 min. After rinsing briefly with water and drying under nitrogen, phosphate-buffered solutions containing 1−2 mM amine-terminated DNA were hand-spotted onto the surface at a volume of 0.5 μL in various patterns. After 2 h in a humidity chamber, the surface was rinsed with distilled water and immersed in 2 M NaCl for 15 min before imaging.

Typically, ethanolamine is applied to surfaces after NHS/EDC-mediated probe attachment in order to "cap" nonreacted carboxylate surface groups that can nonspecifically interact with target molecules such as proteins.[14] We, however, found MUA to sufficiently block the nonspecific binding of actinomycin-D and DNA target molecules (see the Supporting Information, Figure S-3). As a result, ethanolamine "capping" was unnecessary, although we also did not observe nonspecific binding of drug or DNA to ethanolamine-treated surfaces. (Surface treatment with ethanolamine was carried out by exposure of NHS-modified surfaces to 1 M ethanolamine (Sigma-Aldrich), pH = 8.6, for 1 h.)

SPR Imaging Instrument. An SPR imaging instrument using an incoherent white light source was developed for measurement of the kinetics and thermodynamics of biomolecular surface adsorption/desorption and for characterization of biomolecule surface coverage (Figure 1). White light from a short filament 50 W quartz tungsten halogen source is collimated using a 300 μm pinhole filter and passed through a 10 nm band-pass interference filter centered at 633 nm. The generated red light is then directed through a glass slide (used for HeNe laser alignment of the system) and a 500:1 beam-splitting polarizer. This optic selects p-polarized light and passes it through a nematic liquid crystal (LC) variable retarder (LRC-200-VIS-TSC, Meadowlark Optics, Frederick, CO).

The LC variable retarder, discussed below, is used to correct images for spatial intensity variation in the light source as well as time-dependent light intensity fluctuations. After passing through the variable retarder, light is directed into a goniometer-mounted prism onto which a gold-coated slide is coupled by index matching fluid. Images are obtained in air with a trapezoidal BK-7 prism coupled to a microscope slide or in liquid with an equilateral SF-10 prism coupled to an SF-10 glass slide by the appropriate index matching fluid (Cargille Laboratories, $n = 1.5150$ and $n = 1.7300$, respectively). The goniometer controls the incident angle of light, θ, impinging on the patterned film. The reflected image is centered and focused onto a 12-bit CCD camera (512 × 768 pixel) mounted on a rotational arm to accommodate changes in reflected angle. The CCD camera (SenSys, Photometrics), as well as the LC variable retarder, is controlled through custom-written MATLAB software.

The LC variable retarder is employed to correct images for spatial intensity variation in the light source. On the basis of the potential applied to the liquid crystal, the amount of retardation is controlled to generate s- and p-polarized light. The variable retarder is calibrated using crossed polarizers for 0 λ (p-polarized light) and $\lambda/2$ retardation (s-polarized light). Because s-polarized light does not excite surface plasmons, image contrast arises only from the spatial intensity profile of the light beam. Corrected images are therefore obtained through the pixel-by-pixel ratio of p- to s-polarized light images. The images are acquired in sequence (p followed by s) with camera exposure times of 1 s and a polarization switching time of 100 ms.

Figure 2 demonstrates image correction by our instrument. The sample is a commercial SF-10 gold-coated patterned surface (GenTel BioSurfaces, Inc.) with a mercaptoundecanol (MUD) background and patterned 500 × 500 μm squares containing mercaptoundecanoic acid (MUA). The MUA squares are coated with an electrostatically bound poly-L-lysine (PL) layer, which is, in turn, coated with a poly-L-glutamate (PG) layer. The images displayed were obtained in distilled water using an SF-10 equilateral prism; the surface was sealed via Kalrez O-ring to an all-Teflon flow cell.

The spatial intensity variation of the light source is displayed by the s-polarized light image (center). A line profile averaged over the indicated rectangular area (30 pixels wide) shows the shape and extent of this intensity variation, which is manifested in the p-polarized light image of the same area (left). These effects are canceled out through the ratio of p- and s-polarized image intensities, resulting in a corrected image (right) plotted in reflectance ratio, $R_{p/s}$.

With this image correction scheme and optical setup, we have easily resolved surface features with dimensions on the order of hundreds of

(13) Wilkop, T.; Wang, Z. Z.; Cheng, Q. *Langmuir* **2004**, *20*, 11141−11148.

(14) Lahiri, J.; Isaacs, L.; Tien, J.; Whitesides, G. M. *Anal. Chem.* **1999**, *71*, 777−790.

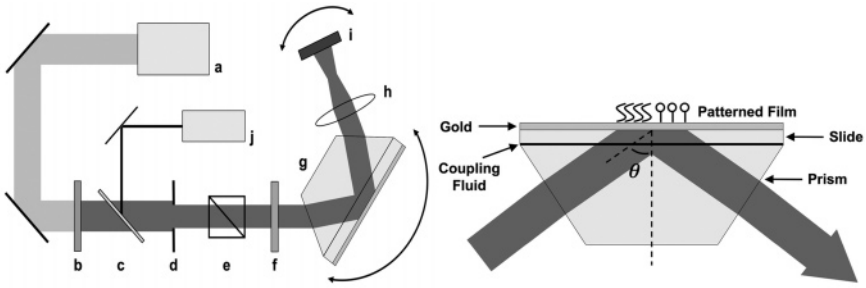

Figure 1. SPR imaging instrument schematic: (a) collimated white light source, (b) band-pass interference filter, (c) glass slide for alignment, (d) iris (1 cm diameter), (e) beam-splitting polarizer, (f) nematic liquid crystal variable retarder, (g) goniometer-mounted prism and patterned slide, (h) focusing lens, (i) CCD camera, and (j) HeNe alignment laser.

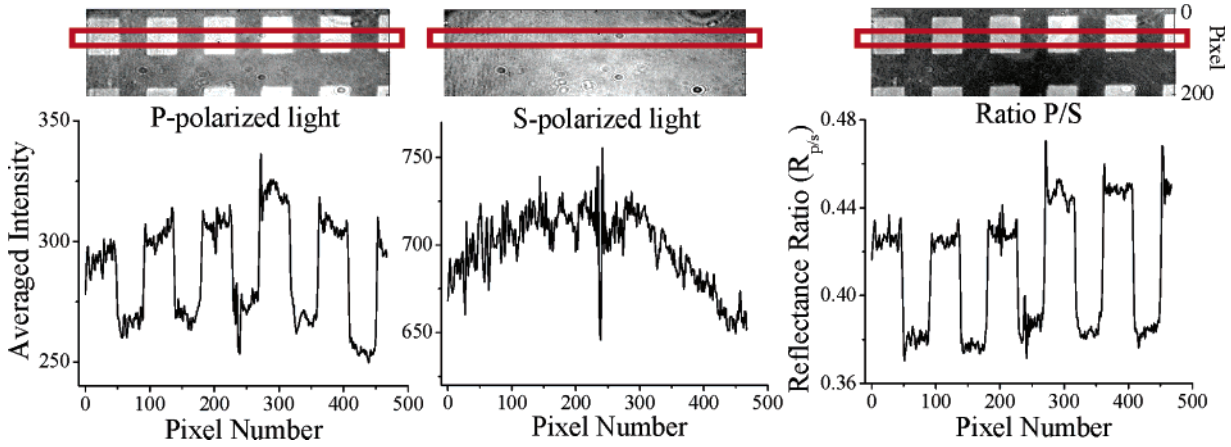

Figure 2. Demonstration of image correction using light polarization as controlled by the nematic liquid crystal variable retarder. The corrected reflectance image (right) was obtained through pixel-by-pixel ratio of p- and s-polarized light images. Averaged line profiles over indicated rectangular areas (30 pixels wide) demonstrate the extent of image correction. See text for details on surface. Images taken in distilled water at 56.3°. Only partial images (200 × 500 pixel regions out of 512 × 768 pixels) are shown for clarity.

microns (500 × 500 μm for commercial surfaces). We have also imaged robotically generated spots of fluorescently labeled DNA on gold with a diameter of 150 μm (see the Supporting Information, Figure S-1). The corresponding 15 pixel diameter indicates that our lateral resolution is limited by our current optical setup rather than by the surface plasmon coherence length. Greve and co-workers, using a similar image correction method and generating p- and s-polarized light via Pockels cell, experimentally determined a lateral resolution of 7 μm for 633 nm light.[15] If necessary, we could easily image smaller features by using different optics to magnify the reflected image.

Angle-Resolved SPR Imaging. By varying the incident angle of light entering the prism and collecting p- and s-polarized light images at each angle, we generate SPR reflectance curves for desired regions of interest akin to those normally acquired by traditional single-spot angle-scanning SPR instruments. At each angle, a corrected image is obtained and analyzed in the same selected regions. Figure 3A demonstrates angle-resolved SPR imaging for the same surface as Figure 2. Each reflectance point corresponds to the average of three 30 × 30 pixel regions of interest (indicated by the dashed boxes in the corrected image at right) in either the background or patterned square areas.

In general, we characterize probe surfaces by fitting angle-resolved reflectance curves to a five- or six-phase Fresnel optical model.[16,17] By combining optical thicknesses and experimentally measured values of refractive index increment, dn/dc, for the DNA adsorbates in the submonolayer, DNA coverage (molecules/cm^2) is calculated from the best fit as demonstrated previously.[18] The six possible phases considered in fitting the data are the glass prism, the thin chromium adlayer, the gold film, the alkanethiol MUD or MUA monolayer, the probe layer, and the solvent. To fit the background curve, we use a five-phase model, assume d_{film} = 17 Å and ϵ_{film} = 1.96 for the alkanethiol (MUD or MUA) layer,[19] and extract optical constants and thicknesses for the chromium and gold layers. These values are then applied to fitting the reflectance data obtained from the patterned probe spots. For six-phase fitting of DNA probe submonolayers, we assume $\epsilon_{DNA\ layer}$ = 2.0.[18]

Six-phase Fresnel model fitting was applied to the angle-resolved imaging curves in Figure 3A. Assuming ϵ_{PL-PG} = 2.31,[19] we obtained an optical thickness of 11.2 ± 0.1 Å for the "probe" PL−PG layer. This value was consistently measured for the commercial surface over the course of months; it is in reasonable agreement with thicknesses determined by traditional angle-scanning SPR for single PL−PG layers at pH <6 given sample age and variation in fabrication.[20]

Kinetic Measurements. In the kinetic experiments discussed in this paper, percent changes in reflectance, % ΔR, are monitored over time at a fixed angle in the selected regions of interest for both the background and probe spots. Binding results are obtained through the region-averaged subtraction of background from probe spot over time. This subtraction corrects for any bulk refractive index changes caused by temperature or concentration variation in solution during the experiment.

The fixed angle chosen to monitor binding kinetics is optimized to report the maximum change in reflectance for each system studied. For instance, Figure 3B demonstrates an optimum angle of 56.3° at

(15) Berger, C. E. H.; Kooyman, R. P. H.; Greve, J. *Rev. Sci. Instrum.* **1994**, *65*, 2829−2836.
(16) Peterlinz, K. A.; Georgiadis, R. *Langmuir* **1996**, *12*, 4731−4740.
(17) Georgiadis, R.; Peterlinz, K. P.; Peterson, A. W. *J. Am. Chem. Soc.* **2000**, *122*, 3166−3173.
(18) Wolf, L. K.; Gao, Y.; Georgiadis, R. M. *Langmuir* **2004**, *20*, 3357−3361.
(19) Jordan, C. E.; Frutos, A. G.; Thiel, A. J.; Corn, R. M. *Anal. Chem.* **1997**, *69*, 4939−4947.
(20) Cheng, Y. F.; Corn, R. M. *J. Phys. Chem. B* **1999**, *103*, 8726−8731.

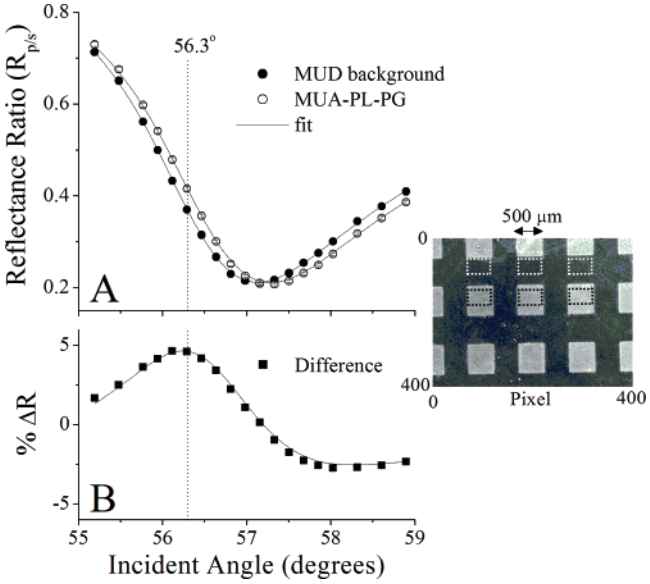

Figure 3. (A) Angle-resolved SPR imaging curves obtained for the same surface as Figure 2. Each point represents the average of three 30 × 30 pixel regions of interest for the MUD background or MUA-PL-PG patterned squares. These regions of interest are indicated by the dashed boxes in the corrected image at right. Solid lines are fits to the data. Error bars represent average variation for the three regions analyzed. The measured angle shift of 0.156° corresponds to a PL−PG layer thickness of a ∼11 Å determined by a six-phase Fresnel calculation. Surface imaged in distilled water (pH = 5.7−5.8). (B) Angle-resolved reflectance difference for the MUD background and MUA-PL-PG patterned squares. The angle of maximum reflectance difference for this system is 56.3° (maximum % Δ*R* of ∼4.5). The solid line is derived from the subtraction of fitted data in A.

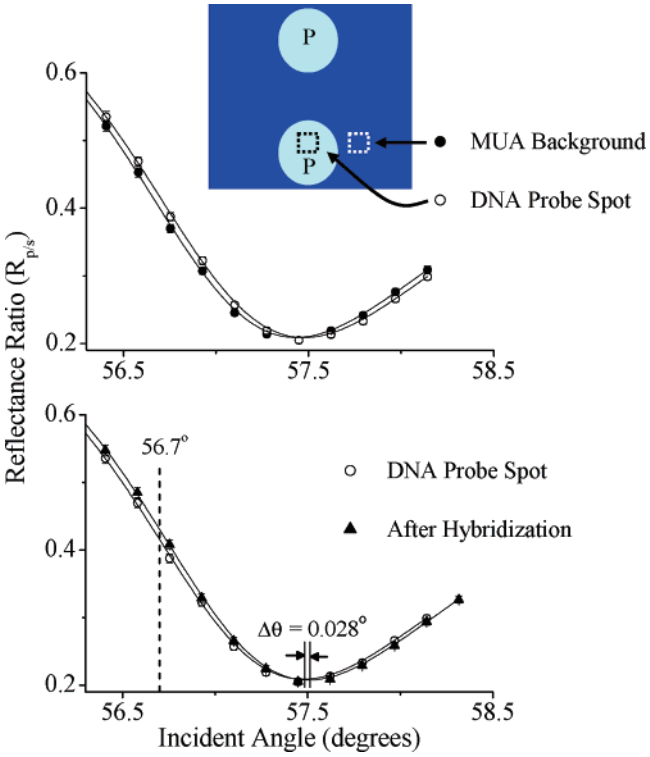

Figure 4. (Top) Angle-resolved imaging data obtained for the patterned DNA probe surface depicted by the inset schematic. The two spots indicate areas of DNA linked via amide bond to the underlying MUA film (hand-spotted at 0.5 μL). Each data point represents DNA spot (open circle) or MUA background (closed circle) and is derived from averaging over 40 × 40 pixel regions of interest (represented by dashed boxes) in the image taken at each angle. (Bottom) Angle-resolved imaging data for the same DNA probe spot before (open circle) and after (closed triangle) hybridization of 1 μM complementary DNA, C. Kinetics of hybridization were monitored at the angle of maximum reflectance difference indicated, 56.7°. Solid lines are fits to the data by a six-layer Fresnel optical model. The surface was imaged in 1 M NaCl/TE.

which a maximum reflectance difference of ∼4.5% is obtained for the commercial surface. This is the angle at which the data in Figures 2 and 3 were obtained and shows the greatest image contrast. The hybridization kinetics displayed in Figure 5 were obtained at 56.7°, the angle of maximum reflectance difference determined from angle-resolved imaging before and after DNA target hybridization (Figure 4, bottom). It has been shown that changes in reflectance monitored at a fixed angle of maximum reflectance difference are linearly proportional to changes in surface refractive index over a certain narrow range.[4] Within this range, direct quantitative comparison of measured surface adsorption kinetics is possible. For our imaging system, we find a linear relationship for reflectance changes (% Δ*R*) less than ∼1.5% and refractive index changes (Δ*n*) less than ∼0.07 (see the Supporting Information, Figure S-2). The refractive index changes associated with the DNA hybridization and drug binding events investigated here fall well within this range, enabling direct measurement and quantitative analysis of these adsorption kinetics.

In addition, we have estimated a limit of detection (LOD) for our imaging system based on this theoretical calculation. Figures 5 and 7 show an average ∼0.05% Δ*R* noise for two 40 × 40 pixel regions of interest, which corresponds to an LOD of Δ*n* ∼ 0.002. The limit of detection is presented as differential refractive index because this unit of measure is general and can be compared to other systems. More specifically, this LOD indicates that our imaging system is capable of detecting down to less than a femtomole of target DNA hybridizing to a 400 × 400 μm probe spot. If necessary, this limit of detection can be further optimized by monitoring larger probe regions or by adjusting, but not redesigning, our current optical setup.

Hybridization and Drug Binding. All DNA hybridizations were carried out at 1 μM DNA target strand concentration in 1 M NaCl/TE. The probe surface was regenerated for subsequent hybridizations by rinsing with copious amounts of SDS (0.4 wt %) and distilled water. Actinomycin-D studies were carried out by first hybridizing the probe surface with the DC strand (perfect complement of the drug binding probe sequence D). The surface was then briefly rinsed with 1 M NaCl/TE (no loss of DC is observed at this ionic strength), followed by injection of an ACTD solution. After approximately 20 min, the solution was replaced with buffer, and drug dissociation was monitored. For subsequent drug bindings, the surface was regenerated by SDS and rehybridized with strand DC.

Results and Discussion

Detection of DNA Hybridization. Figure 4 (top) displays angle-resolved imaging data for the DNA probe surface fabricated for hybridization studies. The surface was patterned without the need for robotic instrumentation by hand-spotting amine-terminated DNA probe (P) onto a MUA film modified by standard EDC/NHS chemistry. Depicted by the inset schematic, the resultant surface consists of a MUA background patterned with two amide-linked DNA spots. We find the MUA background to efficiently block the nonspecific adsorption of DNA (see Supporting Information, Figure S-3), enabling effective background subtraction during hybridization studies.

Fitting of the reflectance data obtained by angle-resolved imaging (one set shown at the top of Figure 4 for the indicated regions of interest) yields an average probe DNA coverage (for both DNA spots) of 2.3 (± 0.1) × 10^{12} molecules/cm^2. This relatively low probe density film (corresponding to an angle shift of 0.045°) is easily resolved by our SPR imaging system. On the basis of established alkanethiol binding geometries,[21]

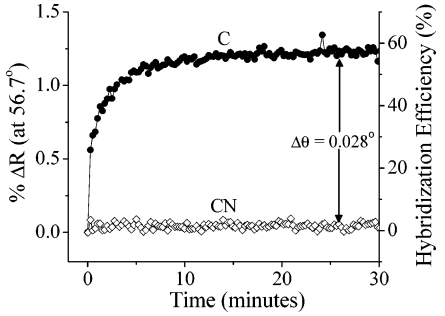

Figure 5. Background-corrected average kinetics of hybridization for two DNA probe spots. The control strand (CN, open diamonds) shows no hybridization at 1 μM (no nonspecific binding). After 30 min, the complementary strand hybridization reaches (1.2 ± 0.2)% ΔR or (57 ± 6)% hybridization efficiency, which correlates to the observed angle shift, 0.028° (shown in Figure 4, bottom). Complementary and control hybridizations were performed on the same SDS-regenerated surface. All hybridizations were carried out in 1 M NaCl/TE.

the surface coverage of MUA on gold is $4.7-4.9 \times 10^{14}$ molecules/cm^2, indicating a coupling efficiency for our system of approximately 0.5%. This low efficiency is typical of the NHS/EDC chemistry used because of competitive NHS hydrolysis[22] and is ideal for producing the low probe density surfaces desired for our studies.

DNA target strand hybridization to this low density surface was also measured and characterized by angle-resolved imaging. Figure 4 (bottom) displays angle-resolved reflectance data for the same DNA probe region of interest before and after complementary strand hybridization. The angle shift observed, 0.028°, correlates to a change in reflectance of 1.2 ± 0.2% observed during time-dependent fixed-angle measurements (Figure 5) and a change in refractive index of ~0.055. Significant complementary strand (C) hybridization was detected, while no binding of the control strand (CN) was observed for the same SDS-regenerated surface.

The hybridization data displayed in Figure 5 are also plotted as a function of percent hybridization efficiency. Hybridization efficiency can be determined by two methods. The first is by fitting of the angle scans before and after hybridization to obtain coverage. The second is by direct ratio of differential refractive index (Δn) between DNA spots and MUA background before and after hybridization. These Δn values are calculated based on measured values of % ΔR and the relationship between changes in refractive index and reflectance determined for our system (see Supporting Information, Figure S-2). We find these methods to agree when the reflectance data before and after hybridization are well-fit (residual of fit <0.003) by the Fresnel optical model. For instance, the single DNA probe spot data in Figure 4 (bottom) yield 61% hybridization efficiency by SPR fitting (fit residual = 0.001) and comparison of differential refractive index. For both probe DNA spots monitored during hybridization, we find an average efficiency of 57 ± 6%. This value compares favorably with efficiencies of 50 and 72% measured on similar probe density surfaces (2×10^{12} and 3×10^{12} molecules/cm^2, respectively) of identical DNA sequence characterized by traditional angle-scanning SPR in the past.[23]

To our knowledge, no comparison of kinetic and thermodynamic results obtained by both angle-scanning and imaging SPR has ever been made for the same system. Figure 6, however, compares the kinetics of DNA hybridization monitored by our imaging instrument with those monitored on a conventional instrument. The same probe and target sequences (P and C, respectively) were employed in both cases, although their surface attachment varied.

The surface schemes in Figure 6 display the two types of surface architecture used: direct attachment of thiolated DNA to gold with mercaptohexanol backfill (scheme 6B) and amine-terminated DNA chemically linked to MUA as described previously (scheme 6A). Architecture B was used in conjunction with the single-spot angle-scanning instrument, while architecture A has been used exclusively with the imaging instrument in the probe spots. Despite the differences in surface architecture and instrumental setup, we find excellent agreement in the measured hybridization kinetics for the same probe−target combination. Figure 6 displays the normalized results of two reproducible hybridizations (open and closed circles) on the same SDS-regenerated array surface as well as a normalized hybridization (red diamonds) measured by a conventional angle-scanning instrument in our laboratory.[23] We have shown previously that hybridization kinetics can be drastically affected by DNA surface probe density. Here, it is worth noting that the probe densities for these surfaces are very similar ($2-3 \times 10^{12}$ molecules/cm^2) and yield the same hybridization kinetics despite different attachment schemes. This result implies that DNA hybridization rate is independent of probe proximity to the surface. While this is not unexpected for well-designed surfaces of appropriate probe density and accessibility, there are contradictory voltammetry results in the literature.[24]

Detection of DNA−Drug Binding. Most SPR imaging studies have measured kinetics for the surface adsorption and desorption of large molecules, such as proteins for which signals are inherently strong.[7,9] We have studied the kinetics of smaller molecule binding to DNA and present the first imaging results for such a system. For this demonstration, we have used a model drug compound, actinomycin-D.

Actinomycin-D (MW = 1255.4 g/mol), an antitumor drug, has been shown to reversibly bind to double-stranded DNA through intercalation.[25] It has also been shown that actinomycin binds specifically to 5′-GC-3′ sites and negligibly to poly(dA-dT) DNA.[26,27] As displayed in Figure 7, we measured actinomycin binding to each of these types of sequences. To do so, we used the surface fabrication methods discussed previously, and hand-spotted amine-terminated poly(dT) and an amine-terminated strand containing three identical drug binding sites (D) onto a surface. The surface image before hybridization is displayed in the inset of Figure 7. The top two amide-linked DNA spots contain poly(dT), while the bottom two spots contain strand D. Analysis of SPR curves generated for the spots and backgrounds in the selected regions of interest yielded similar probe densities for the D and poly(dT) strands ($2.8 \pm 0.2 \times 10^{12}$ and $2.4 \pm 0.4 \times 10^{12}$ molecules/cm^2, respectively), suggesting that sequence composition has little effect on coupling efficiency to the monolayer surface. In contrast, we have recently shown strong dependence of DNA immobilization coverage on sequence composition caused by nonspecific

(21) Strong, L.; Whitesides, G. M. *Langmuir* **1988**, *4*, 546−558.
(22) Gong, P.; Grainger, D. W. *Surf. Sci.* **2004**, *570*, 67−77.
(23) Peterson, A. W.; Heaton, R. J.; Georgiadis, R. M. *Nucleic Acids Res.* **2001**, *29*, 5163−5168.
(24) Wong, E. L. S.; Chow, E.; Gooding, J. J. *Langmuir* **2005**, *21*, 6957−6965.
(25) Muller, W.; Crothers, D. M. *J. Mol. Biol.* **1968**, *35*, 251−290.
(26) Jain, S. C.; Sobell, H. M. *J. Mol. Biol.* **1972**, *68*, 1−20.
(27) Chen, F. M. *Biochemistry* **1988**, *27*, 6393−6397.

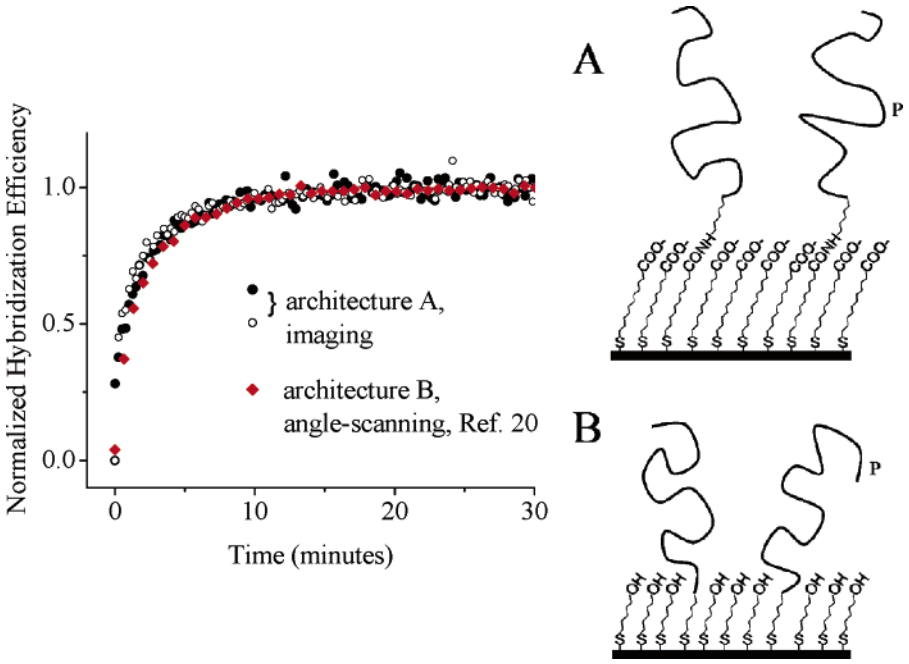

Figure 6. Hybridization efficiency normalized at 30 min for 1 μM target hybridizations on two different systems. Two consecutive hybridizations on the same SDS-regenerated patterned surface previously discussed were measured with our SPR imaging instrument (open and closed circles). These hybridizations were carried out on the surface architecture depicted in scheme A. Hybridization of the same target sequence (C) to the same probe sequence (P) was also measured by a conventional angle-scanning instrument (ref 20). This measurement (red diamonds) was carried out on the surface architecture depicted in scheme B. Both surfaces investigated had similar probe densities ($2-3 \times 10^{12}$ molecules/cm^2). Measurements were all carried out in 1 M NaCl/TE.

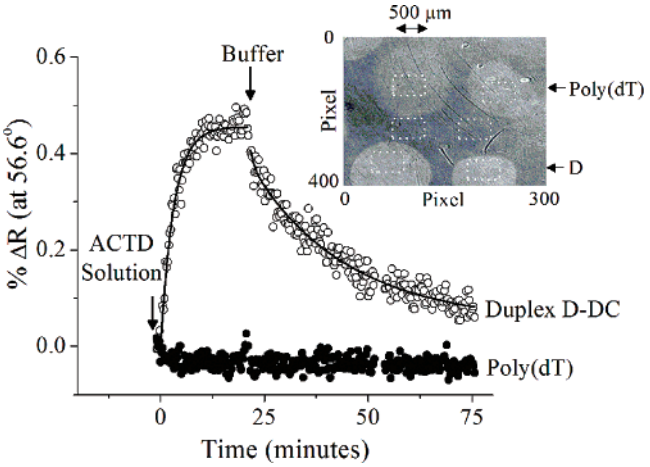

Figure 7. Background-corrected average binding kinetics of 1 μM actinomycin-D in 1 M NaCl/TE to the hand-spotted DNA surface indicated by the inset image. The top two spots in this prehybridization image contain poly(dT), while the bottom two spots contain strand D. During analysis of probe density and interaction kinetics, the left-hand background region of interest was applied to the DNA spots in the left-hand column, while the right-hand background was applied to the DNA spots in the right-hand column. All regions were 40 $\times$ 40 pixels in dimension. Drug solution was injected at $t = 0$ and replaced by pure buffer (1 M NaCl/TE) at $t = 20$ min. All results shown were measured in parallel. No drug binding was observed for single-stranded poly(dT) spots (closed circles). Clear association and dissociation of drug to and from duplex DNA (D-DC) spots (34 $\pm$ 5% hybridization efficiency for this cycle) was observed (open circles). Lines are a guide to the eye.

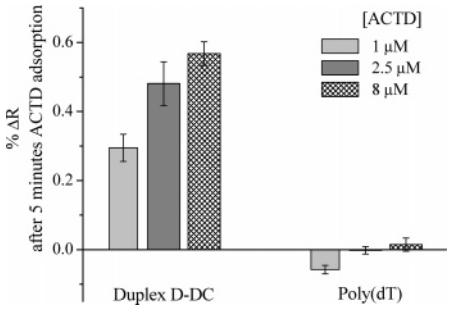

Figure 8. Values of background-corrected % ΔR measured after 5 min of actinomycin association for varying concentrations. Binding is only observed for the spots containing duplex DNA D-DC. This binding increases with drug concentration as expected. No drug binding is observed for poly(dT) even at the highest concentration. Error bars represent spot-to-spot variations. These variations for poly(dT) are smaller than the noise of the measurements themselves. The negative change for 1 μM ACTD is most likely caused by imperfect background subtraction. All measurements were carried out in 1 M NaCl/TE.

interaction between DNA nucleotides and the gold surface.[18] Here, the access to the gold surface is blocked by the MUA film, and DNA couples to the surface only through formation of amide bonds with exposed carboxylic acid groups.

Prior to the drug binding represented by Figure 7, the surface was exposed to a solution of the oligonucleotide complement (DC) to the surface-tethered D strand. Hybridization was detected only in the two probe spots containing sequence D (hybridization efficiency of 34 $\pm$ 5%); no binding to the poly-(dT) areas was observed (data not shown). After hybridization, the surface was briefly rinsed with buffer followed by injection of 1 μM actinomycin-D. As displayed in Figure 7, no drug binding to the poly(dT) spots occurred, while significant binding was observed for the double-stranded D-DC spots. After approximately 20 min, the drug solution was replaced by pure buffer, and slow actinomycin dissociation from the duplex DNA was observed. This slow dissociation has significance, as it correlates to the role actinomycin-D plays in disrupting the transcription process.[25]

A number of drug association/dissociation cycles were monitored for this same surface after SDS regeneration and rehybridization. Figure 8 displays the values of % ΔR after 5 min of drug association at different concentrations on similar

duplex DNA surfaces (average DC hybridization efficiency for these surfaces was 31 ± 6%). For the double-stranded D-DC spots, the values follow the expected trend, increasing with concentration as association rates increase. For the single-stranded poly(dT) spots, there is no significant binding even at the highest concentration. The MUA background efficiently blocks nonspecific adsorption of drug (Supporting Information, S-3).

Quantitation of drug binding is achieved through the comparison of changes in refractive index for DNA hybridization (Δn_{HYB}) and actinomycin (Δn_{ACTD}) adsorption. The standard coverage calculation equation[18] is adapted into a proportion as follows:

$$r = \left\{\frac{\Delta n_{ACTD}}{\left(\frac{dn}{dc}\right)_{ACTD} \times MW_{ACTD}}\right\}\left\{\frac{\left(\frac{dn}{dc}\right)_{HYB} \times MW_{HYB}}{\Delta n_{HYB}}\right\}$$

where r is the number of actinomycin molecules bound per DNA duplex, and MW_{HYB} and MW_{ACTD} are the molecular weights of strand DC and actinomycin-D, respectively. The refractive index increment for DNA, $(dn/dc)_{HYB}$, was measured previously[18] and for actinomycin-D, $(dn/dc)_{ACTD}$, was found to be 0.256 ± 0.004 measured in methanol by the same method. Using saturated Δn values (at ~20 min) for both the 1 μM actinomycin adsorption (Figure 7) and corresponding DNA hybridization in this proportion yielded 2.9 ± 0.1 actinomycin-D molecules per DNA duplex. This result suggests that 1 μM drug completely saturates the available duplex drug binding sites on the surface, corresponding to the three sites present in the designed duplex D-DC. These results indicate that our imaging instrument easily enables the quantitative measurement of kinetics and thermodynamics for DNA−drug interactions. Further analysis of kinetics and thermodynamics for the actinomycin-D system and comparisons to solution-phase measurements are the subject of another publication.[28]

Summary and Conclusions

We have developed an SPR imaging system for measuring biomolecule interactions at surfaces. Using an angle-resolved imaging approach and a surface architecture that blocks nonspecific binding of target molecules, we have quantitatively characterized DNA probe molecule coverage as well as DNA hybridization efficiency. We find excellent agreement between our thermodynamic hybridization imaging results and those obtained for the same probe−target sequence hybridization measured by traditional angle-scanning SPR. In addition, we have detected and quantitatively characterized DNA−drug binding for the first time with SPR imaging. With our current optical setup, we have the sensitivity to measure such changes in refractive index (LOD ~ 0.002) and are able to measure surface features of diameter ~150 μm. These limits can be further optimized for other applications without changing our instrumental design.

We have also measured the kinetics of DNA hybridization and DNA−drug binding by monitoring fixed-angle percent changes in reflectance over time. Despite differences in instrumental setup and surface architecture, we find excellent agreement in the same probe−target sequence hybridization kinetics measured by our SPR imaging instrument and traditional angle-scanning SPR. Additionally, we are able to observe drug association and dissociation from multiple DNA sequences and spots simultaneously. A thorough investigation of the kinetics and thermodynamics of drug binding and comparison to solution-phase measurements is currently underway in our laboratory. This type of comparison may have future implications for the validation of drug candidate biosensing assays.

Acknowledgment. The authors acknowledge financial support from the National Cancer Institute of the NIH (CA 89562), and the National Science Foundation (DBI-0096731). D.E.F. was supported by the Boston University Undergraduate Research Opportunities Program (UROP) and an NSF-REU supplement. This work was partially supported by the Army Research Laboratory (Cooperative Agreement DAAD19-00-2-0004) and resources at the Boston University Photonics Center. The authors thank Professor Scott E. Schaus and his laboratory at Boston University for help with robotic spotting and for their donation of the fluorescently labeled DNA used in this work.

Supporting Information Available: Comparison of fluorescence and SPR imaging of robotically spotted, physisorbed, Cy3-labeled DNA on gold (features ~ 150 μm). Relationship between reflectance and refractive index changes for our SPR imaging system. Experimental details and results of drug and DNA nonspecific binding to mercaptoundecanoic acid control surface. This material is available free of charge via the Internet at http://pubs.acs.org.

(28) Wolf, L. K.; Georgiadis, R. M. Manuscript in preparation.

JA056422W